CHARACTERIZATION OF CONTEXTS FOR RADIOCARBON DATING: RESULTS FROM THE EARLY IRON AGE AT TELL ES-SAFI/GATH, ISRAEL

Michael Toffolo[1,2] • Aren M Maeir[3] • Jeffrey R Chadwick[4] • Elisabetta Boaretto[1]

ABSTRACT. The reliability of a radiocarbon date depends in part on the degree of precision and accuracy of the measurement. While analytical precision and accuracy can be improved by careful sample cleaning procedures and high laboratory standards, accuracy also depends upon the certainty to which the sample can be attributed to a specific material culture or event in the past. This might be questionable when based only on partial archaeological information. As a consequence, it is very difficult to date clear-cut chronological transitions within specific periods. This issue is particularly apparent in the case of Mediterranean Iron Age chronology, where 2 somewhat different perspectives are proposed, the "High Chronology" and the "Low Chronology," which differ by ~50 yr. Here, we present the preliminary results of an ongoing project that aims to characterize Iron Age archaeological contexts from the eastern Mediterranean, and to identify those contexts that are suitable for dating, in order to improve the accuracy of ^{14}C dates. This study involves the analysis of sediments by means of FTIR spectrometry, soil micromorphology, phytolith and phosphate extraction, all of which provide insights into the site-formation and postdepositional processes at the different sites under investigation. These techniques, applied at Tell es-Safi/Gath (Israel), enabled us to better identify a secure context for dating.

INTRODUCTION

The transition between the Late Bronze Age and Iron Age in the eastern Mediterranean is one of the most interesting cultural phases in the history of the Mediterranean. Various processes, changes, and new directions are attested during this period, including the fall and weakening of various important polities and cultures (e.g. the fall of the Hittite empire; the destruction of the Mycenaean palaces; the appearance of new cultures, such as the Sea Peoples, the Israelites, the Arameans, etc.), along with major shifts in the socioeconomic fabric(s) in a very wide region (Ward et al. 1992; Gitin et al. 1998; Killebrew 2005; Harrison 2006–2007; Bachhuber and Roberts 2009). One such event is the appearance of the Philistines, apparently one of the so-called "Sea Peoples," whose archaeological correlates are manifested in the southern Coastal Plain of present-day Israel/Palestine, in the region often termed "Philistia." At various sites in this region, distinct material culture attributes appear during the Late Bronze/Iron Age transition, which indicate the appearance of non-local influences and peoples, apparently originating from the Aegean, Cyprus, and SE Europe. This includes the appearance of locally made Late Helladic IIIC pottery, along with new types of architecture and cultic paraphernalia, changes in diet, and other facets (Oren 2000; Harrison 2006–2007; Yasur-Landau 2010). The exact dating of the appearance of these new cultural attributes has been debated, with the 2 most commonly suggested dates being the early or mid-12th century BCE. These 2 options are related, respectively, to the High Chronology (HC) and to the Low Chronology (LC) for the Iron Age in Israel (see, for example, for the HC: Bruins et al. 2003; Mazar et al. 2005; van der Plicht et al. 2009. For the LC: Finkelstein 1996; Boaretto et al. 2005; Sharon et al. 2007; Finkelstein and Piasetzky 2010). Several sets of radiocarbon dates from many sites located in the southern Levant support the 2 different views on the Bronze Age/Iron Age transition (Mazar and Carmi 2001; Carmi and Ussishkin 2004; Finkelstein and Piasetzky 2007; Sharon et al. 2007; van der Plicht et al. 2009). However,

[1]Radiocarbon Dating and Cosmogenic Isotopes Laboratory, Kimmel Center for Archaeological Science, Weizmann Institute of Science, Rehovot 76100, Israel.
[2]Jacob M Alkow Department of Archaeology and Ancient Near Eastern Civilizations, Tel Aviv University, Tel Aviv 69978, Israel. Corresponding author. Email: Michael.Toffolo@weizmann.ac.il.
[3]Martin (Szusz) Department of Land of Israel Studies and Archaeology, Bar-Ilan University, Ramat-Gan 52900, Israel.
[4]Jerusalem Center for Near Eastern Studies, Brigham Young University, Provo, Utah 84602, USA.

Proceedings of the 6th International Radiocarbon and Archaeology Symposium, edited by E Boaretto and N R Rebollo Franco
RADIOCARBON, Vol 54, Nr 3–4, 2012, p 371–390

the numerous wiggles in the calibration curve for this period, problematic stratigraphic correlations, poor attention to sampling methodology and context characterization, and the choice of long-lived samples (such as wood charcoal) limited the precision and accuracy of the measurements, thus hampering the definition of a clear-cut transition (see, for instance, the debate on the stratigraphy of Tel Dan in van der Plicht et al. 2009; Bruins et al. 2011; Fantalkin et al. 2011; see also, for more general considerations, van der Plicht and Bruins 2001; Boaretto 2009).

The excavations at Tell es-Safi/Gath (Maeir 2008, 2012; Figure 1) have produced extensive evidence of various stages of the Philistine culture, from its first appearance in the early Iron Age until the Iron Age IIA. In recent seasons, several early Philistine contexts have been excavated. In the current study, an attempt was made to define the robustness, from a microstratigraphic point of view, of one of these early contexts. Once a secure stratigraphic context could be determined, carbonized botanical remains were processed for ^{14}C dating. The importance of this methodology is that it can provide a clear and well-defined series of absolute dates for the earliest appearance of the Philistine culture in this and other sites in Philistia. On a wider scale, the dates obtained through this methodology could be used as a chronological peg for the transition between the Late Bronze Age and the Iron Age in the southern Levant in general.

Figure 1 Map of Israel with the location of Tell es-Safi/Gath and other major Iron Age sites.

https://doi.org/10.1017/S0033822200047159 Published online by Cambridge University Press

Due to the importance of dating this transitional stage, it was essential to try and demarcate extremely well-defined stratigraphic contexts—contexts from which one can be quite sure that the carbonized remains are from primary deposition, and not from redeposited sediments. Since the identification of secure contexts is often difficult by just observing the stratigraphy, a more accurate point of view at the microscale level is required. Therefore, we decided to use the scientific approach described in Weiner (2010), which includes different analytical methods. Each one of these addresses a different aspect of the context, but combined altogether they can provide a reliable picture of the formation processes involved in the genesis of the stratigraphy.

This improved methodology can increase the degree of accuracy of the measurements by defining a clear and strong link between the sample that is going to be dated and the pottery assemblage and specific human activity that led to its deposition in the stratigraphic sequence (e.g. occupational accumulation on floor, tabun, hearth, storage vessel with seeds, destruction event, phytolith layer, etc.).

Archaeological Context

The samples for this study were from Locus 126405, an assumed domestic surface (floor) of a small room excavated in Area F in Tell es-Safi/Gath. Surface 126405 was the uppermost of a series of 4 early Iron Age I surfaces excavated during the 2009 and 2010 seasons in Square 16C of Area F (Figures 2–3). These were all beaten-earth floors, one superimposed atop another in a vertical accumulation 40 cm high. Three of the surfaces yielded ceramic sherds of decorated, locally made Philistine Mycenaean IIIC pottery (also known as "Philistine 1," see Maeir 2005) as the latest datable samples. These ceramics featured monochrome designs typical of the repertoire known from Stratum VII at Tel Miqne/Ekron (Dothan and Zukerman 2004; Dothan et al. 2006), which suggests that the surfaces should be dated to the early Iron Age I period, specifically the 12th century BCE—the initial decades of the Philistine occupation of Tell es-Safi/Gath after the transition from Canaanite control at the end of the Late Bronze Age (Table 1). The ceramic samples from Surface 126405 (Figure 4) were all sherds of fine thin ware with a monochrome decoration in the form of thin red lines, painted horizontally onto the vessel surface. The samples represented at least 4 different vessels, 2 of which were certainly small bell-shaped bowls (*skyphoi*), and the other 2 most probably small bell-shaped bowls. By the excavator's estimation, Surface 126405, as the latest of the early Iron Age I floors, would have been in use in the late 12th century BCE, and possibly also in the early 11th century BCE.

Figure 2 View of Area F at the end of the 2009 excavation season and associated relative chronology. The arrow marks the location of Square 16C.

https://doi.org/10.1017/S0033822200047159 Published online by Cambridge University Press

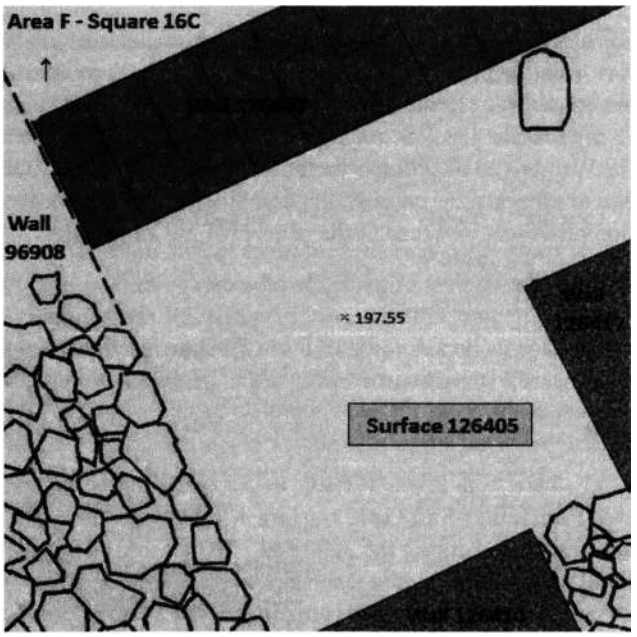

Figure 3 Reconstruction of the room of Square 16C (arrow marks north)

Table 1 Iron Age I surfaces excavated in Square 16C of Area F at Tell es-Safi/Gath.

Surface locus	Level	Year	Stratum	Latest sherds
Surface 106405	197.70	2007	FL-1 later Iron I	Iron I Bichrome
Surface 126405*	197.55	2009	FL-2 early Iron I	Iron I Myc IIIC
Surface 126409	197.45	2009	FL-2 early Iron I	Iron I generic
Surface 126413	197.35	2009	FL-2 early Iron I	Iron I Myc IIIC
Surface 136409	197.17	2010	FL-2 early Iron I	Iron I Myc IIIC

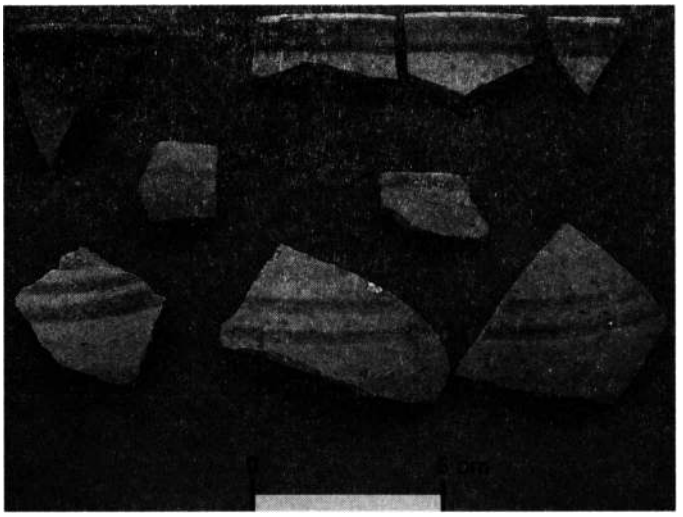

Figure 4 Mycenaean IIIC ceramic samples from Locus 126405

https://doi.org/10.1017/S0033822200047159 Published online by Cambridge University Press

Area F includes a segment of the ancient city fortification (Wall 96908), which, based on ceramic evidence, was constructed during the Middle Bronze Age II (~1750–1550 BCE), and was in use until at least the end of Iron Age I (~980–960 BCE according to the HC [Mazar et al. 2005; van der Plicht et al. 2009]; ~920–900 BCE according to the LC [Finkelstein and Piasetzky 2010]). The floors excavated in Square 16C, including Surface 126405, belonged to a room located just inside the city wall line. The inside face of the city wall's brick superstructure apparently served as the western interior wall of this room. Two narrower walls, more typical in size for domestic structures, formed the southern and eastern borders of the room. They were constructed of a composite adobe (rather than brick), apparently during the Late Bronze Age (1550–1200 BCE), and were numbered by the excavators as Walls 126414 and 126417. Based on ceramic evidence, the room itself was apparently in use as early as the Late Bronze Age, long before the construction of the early Iron Age I floor layers. At the outset of Iron Age I, the barrier that formed the north limit of the room was overlaid with a wall of mudbricks. This mudbrick wall was numbered Wall 126407 by the excavators, and it stood throughout the duration of the Iron Age I surfaces of Square 16C. In addition to the architectural archaeological settings, the following observations support the notion that Locus 126405 represents an archaeological context suitable for ^{14}C dating:

1. The presence of small white patches composed of siliceous phytoliths still organized as fibers that reflect the imprints of the original plant material.
2. The phytoliths are associated with charred material, such as charcoal and olive pits.
3. Pottery fragments are arranged horizontally on the surface.

MATERIALS AND METHODS

The analytical methods used were aimed at understanding the depositional mode of the surface, its preservation and degree of bioturbation, and for tracing possible signals of anthropogenic activity (Boaretto 2007, 2009; Weiner 2010). The indicators used are phosphate content, phytolith morphology, heat-altered sediments, and formation processes.

Phosphates within archaeological sediments are related to the decay of organic material and, therefore, can indicate the presence of areas of past human activities (Holliday and Gartner 2007). Phytoliths are mineral components produced by many plants. They are composed mainly of calcium oxalate (CaC_2O_4), amorphous calcium carbonate (ACC, also known as cystoliths), and opal, an amorphous form of SiO_2 (Mulholland and Rapp 1992; Piperno 2006). However, only the opaline phytoliths are preserved in archaeological settings. Their importance in archaeological contexts is related to the fact that plant organic tissues are often not preserved in archaeological deposits; thus, phytoliths are the only "fingerprint" available to reconstruct the vegetal environment. The study of phytoliths within sediments can help in identifying floors and occupation surfaces, activity areas, and fuel types.

Fourier transform infrared (FTIR) spectrometry is a basic tool for the study of sediments because it gives a qualitative analysis of the different chemical phases (both organic and inorganic) occurring in the sample. It can also detect the presence of phosphates, of heat-affected sediments (Berna et al. 2007), and differentiate between geogenic (e.g. limestone) and anthropogenic calcite (e.g. ash and lime-plaster; Chu et al. 2008; Regev et al. 2010a,b). Therefore, it can provide information about the presence of activity areas, such as hearths, or the presence of lime-plaster floors.

Finally, archaeological soil micromorphology is based on the observation and description of soil thin sections (30 μm in thickness) with a polarizing microscope (Bullock et al. 1985; Stoops 2003). Micromorphology is particularly useful in the identification of floors and occupation surfaces, but

also for other types of archaeological features, and it is invaluable for determining the site-formation processes (depositional and postdepositional) that took place in a specific context, thus allowing the distinction between *in situ* and non-*in situ* deposited sediments (Courty et al. 1989; Goldberg and Macphail 2006; Goldberg and Berna 2010).

Fourier Transform Infrared (FTIR) Spectrometry

Samples (n = 25) were collected from the surface and through the thickness of the occupational accumulation (~10 cm). A few milligrams of the sample were homogenized and powdered in an agate mortar and pestle. Approximately 0.2 mg were left in the mortar and mixed with ~40 mg of KBr (IR-grade) and pressed into a 7-mm pellet using a hand press (Qwik Handi-Press, Spectra-Tech Industries Corporation) or a manual hydraulic press (Specac). Infrared spectra were obtained at 4-cm^{-1} resolution for 32 scans, between 4000 and 250 cm^{-1}. FTIR analyses on-site were made using a Nicolet IR200 (Thermo) spectrometer, or in the laboratory using a Nicolet 380 (Thermo). The heights of the ν2 and ν4 peaks of calcite were normalized to the height of the ν3 peak, and their ratio calculated, following the method of Chu et al. (2008). The full width at half maximum (FWHM) of the ν3 peak was used to distinguish between different types of calcite (Regev et al. 2010a; Poduska et al. 2011).

Phosphate Analysis

Phosphate concentrations in the sediments were determined during and after the excavation using a modified version of the method of Rypkema et al. (2007). Samples (n = 10) were chosen among those collected for FTIR spectrometry. Approximately 50 mg of sediment from the sample were homogenized in an agate mortar and pestle and placed into a 15-mL tube. Then, 1.5 mL of 1M HCl was added to the sample to dissolve the carbonates. Next, 8.5 mL of Mehlich-3 extracting solution (a mixture of ammonium nitrate, acetic acid, nitric acid, ammonium fluoride and ethyldiamine tetraacetic acid) were added to the sample. The solution was then vortexed and left to cure for 10 min. Then, 1 mL of the solution was removed and transferred into a 1.5-mL Eppendorf tube, and centrifuged for 5 min at 1000 rpm. Next, 20 μL of the supernatant were transferred into a new 1.5-mL tube, together with 980 μL of Mehlich-3 extracting solution. A blank solution with 1 mL of Mehlich-3 was then prepared. Finally, 150 μL of 2 different color reagents were added to the sample and to the blank solution. Reagent A is a solution of sulfuric acid and ammonium molybdate; reagent B is a solution of malachite green and polyvinyl alcohol. Absorbance was measured with an Ocean Optics USB650_ISS_UV/VIS spectrometer at 600 nm.

Phytolith Analysis

Phytolith concentrations in the sediments were determined during and after the excavation using the method of Katz et al. (2010). Again, samples (n = 4) were chosen among the sediments collected for FTIR spectrometry. Approximately 20 mg of homogenized sediment were placed in a 0.5-mL Eppendorf tube and 50 μL of 6N HCl were added to the sample to dissolve the carbonates. Then, 450 μL of sodium polytungstate (2.4 g/mL density) were added and the sample was vortexed, sonicated for 20 min, and centrifuged at 5000 rpm for 5 min. The supernatant was then transferred to another tube, vortexed, and 50 μL of the solution were placed on a slide and covered with a coverglass. Phytoliths were counted at 200× magnification. Phytolith identification was carried out using the standard literature (Twiss et al. 1969; Piperno 1988; Mulholland and Rapp 1992). The International Code for Phytolith Nomenclature was also followed where possible (Madella et al. 2005). The presence of dung spherulites (Canti 1999; Shahack-Gross 2011) in all of the 25 samples collected was checked in the laboratory by mounting the original sediment on a glass slide with Entellan (Merck).

Micromorphology

Two undisturbed sediment blocks were carved out from Locus 126405. Sample TS9517 was taken at the top of the step section dividing the upper and the lower half of Square 16C, whereas sample TS9526 was collected at the boundary between a mudbrick and the top of the locus surface (Figure 5). The samples were prepared for micromorphological analysis following conventional procedures (Courty et al. 1989). The blocks were dried in an oven at 50 °C for 3 days and then impregnated using a mixture of 7 parts of polyester resin and 3 parts of acetone. When hard, the impregnated blocks were cut in slices using a rock saw. The slices were processed into 30 μm thickness, 2 × 3 inch size thin sections by a commercial company (Quality Thin Sections, Tucson, Arizona). The thin sections (n = 6; 3 for each sample) were studied using polarizing light microscopes (Nikon Labophot2-POL and Nikon Eclipse 50iPOL) at various magnifications (20×, 40×, 100×, 200×, and 400×), and with blue fluorescent light (BL). Micromorphological descriptions employ the terminology of Bullock et al. (1985) and Stoops (2003).

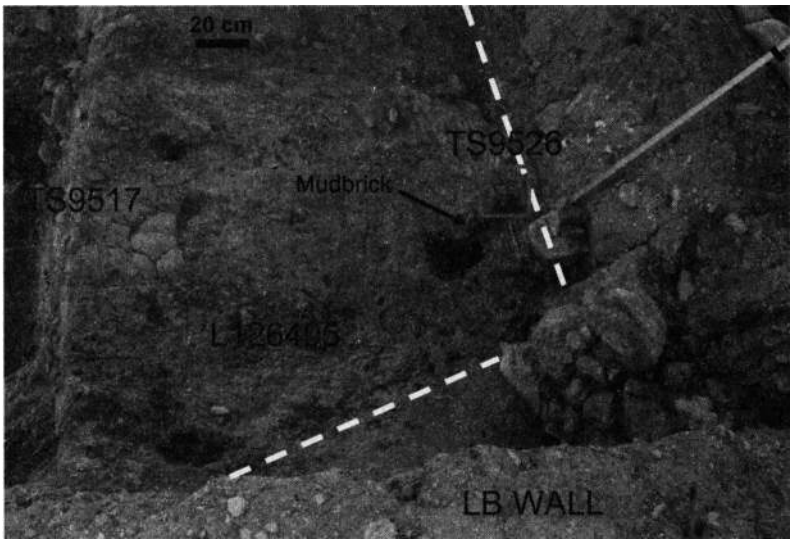

Figure 5 View from above of Locus 126405, Square 16C during the excavation, with the location of the blocks for micromorphology (squares). The dashed line marks the boundary of Locus 126405.

Radiocarbon Dating

Four samples of charred single olive pits and 4 samples of charcoal were collected from Locus 126405 by means of field-picking, and ^{14}C dated after evaluating the results of the above-mentioned methodologies. Because of the novelty of this approach in context characterization, we decided to include in our study also charcoal samples in order to compare the results with short-lived samples, even though one has always to bear in mind a potential old-wood effect.

The material selected for ^{14}C dating was pretreated following Yizhaq et al. (2005) and Rebollo et al. (2008), in order to remove all the carbon-bearing contaminants. Thus, a general acid-base-acid (ABA) protocol was followed (Olson and Broecker 1958). After pretreatment, the samples were analyzed using FTIR spectrometry to determine the purity of the charcoal recovered. Then, the samples were oxidized in vacuum with CuO at 900 °C and prepared as graphite for ^{14}C determination using accelerator mass spectrometry (AMS). All samples provided enough carbon for the AMS

https://doi.org/10.1017/S0033822200047159 Published online by Cambridge University Press

measurement. ^{14}C ages are reported in conventional ^{14}C years before present (BP) following the international convention (Stuiver and Polach 1977). All calculated ^{14}C ages have been corrected for isotopic fractionation based on the stable carbon isotope ratio ($\delta^{13}C$ value). Calibrated ages in calendar years have been obtained from the calibration tables of Reimer et al. (2009) using OxCal v 4.1 (Bronk Ramsey 2009).

RESULTS

Sediment Composition

Calcite is the main component of the sediments of Locus 126405, together with clay minerals, whereas quartz shows only weak absorption bands (Figure 6). According to the methodology proposed by Regev et al. (2010a) for the identification of anthropogenic and natural calcite, the normalized heights of the v2 and v4 peaks and the FWHM of the v3 peak of calcite point in some cases to a pyrogenic origin of this component, in the form of ash. It is interesting to note that the clay minerals do not show any sign of exposure to temperatures above 400 °C (Berna et al. 2007; Eliyahu-Behar et al. 2012). Absorption bands of opaline silica, the material of which phytoliths are composed, were not identified, although it is difficult to discern the 1100-cm^{-1} peak of phytoliths from the peak of clay minerals at 1034 cm^{-1} when their amount is low compared to the clay minerals. Opaline silica might occur just as a weak shoulder on the main clay peak. Weak absorption bands of dahllite (i.e. carbonated apatite [$Ca_5(PO_4)_3(OH)$], a phosphate mineral) at 567 and 604 cm^{-1} were observed. We conclude that there is evidence for human presence as indicated by the phosphates, whereas it is not clear whether the ash-derived pyrogenic calcite is from plants burnt elsewhere at the site and then dumped in Locus 126405, or from plants burnt *in situ*.

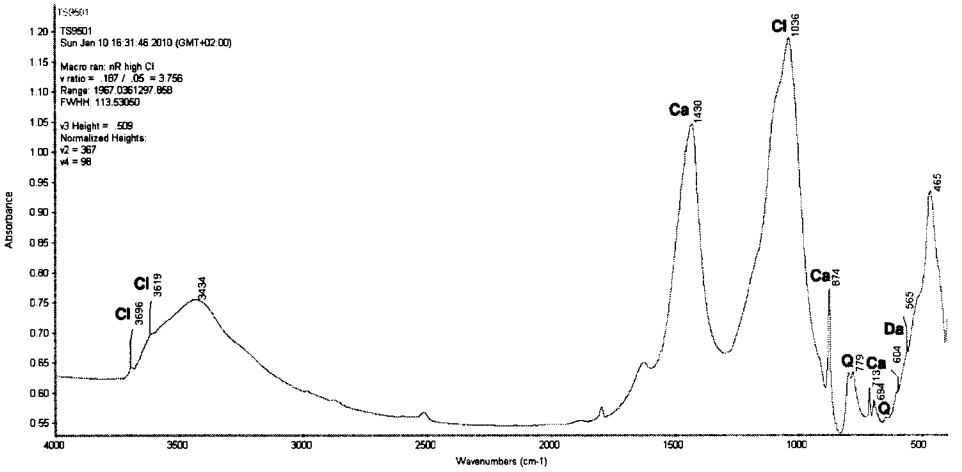

Figure 6 FTIR spectrum of sample TS9501: Cl = clay minerals; Q = quartz; Ca = calcite; Da = dahllite

Phosphate Analysis

The weight percent of phosphates in total sediments ranges between 0.17 and 2.13% (Table 2). The standard deviation error associated with each measurement depends on the optical density (OD) measured for each sample. Based on 3 repetitions of the measurements of different standard phosphate concentrations, we calculated that for OD values between 0.2 and 1, the standard deviation is ±15%. For OD values higher than 1, the standard deviation is ±1%.

https://doi.org/10.1017/S0033822200047159 Published online by Cambridge University Press

Table 2 Weight percent of phosphates on total sediment (* = control sample).

Sample ID	Optical density (OD)	Concentration of phosphates (%)
TS9500	0.12	0.17 ± 15
TS9502	1.15	1.66 ± 1
TS9503	0.98	1.38 ± 15
TS9504	1.22	1.72 ± 1
TS9505	0.94	1.38 ± 15
TS9509	0.66	0.97 ± 15
TS9512	1.34	1.97 ± 1
TS9515	1.48	2.13 ± 1
TS9521	1.22	1.76 ± 1
TS9526*	0.16	0.23 ± 15
TS9527	1.26	1.85 ± 1

The control sample, a mudbrick lying on the surface of Locus 126405, shows a concentration of 0.23% of phosphates. This feature was selected because we assumed that its phosphate concentration would represent an average (background) concentration for the archaeological site, but not related to a specific human activity. Nine out of 10 samples show much higher values compared to the control sample, indicating the presence of high concentrations of phosphates. The very low value shown by sample TS9500 is consistent with the control if we bear in mind that this sample comes from the mudbrick detritus covering Locus 126405. Note that sample TS9527, a fill deposit located ~40 cm below Locus 126405, shows a high concentration of phosphates, even though it is not related to any floor or occupational accumulation. This is an example of sediment that should not be chosen as a control for phosphate analysis.

Phytolith Analysis

Phytolith concentrations and percentages of morphotypes are presented in Table 3. The samples show concentrations of phytoliths per gram that are 2 to 3 times higher than the control sample. The control sample (TS9527) is the fill located ~40 cm below the locus under study. Although a mudbrick could be considered as "sterile" from the point of view of phytolith concentration (i.e. almost devoid of phytoliths) and, therefore, it could be a better control sample, in this case we preferred to rely on a fill deposit, which contains a general phytolith assemblage comparable to the one of other features such as floors, but not directly related to a specific human activity. Thus, this assemblage can be considered as a background.

Table 3 Phytolith concentrations and percentages of different morphotypes (F = festucoids; P = panicoids; C = chloridoids).

Sample ID	Concentration (millions/g of sediment)	Grasses	Dicot	Weathered	Leaf+ stem[a]	Inflore-scence[a]	Dend-ritics	F[b]	P[b]	C[b]	Multi cells
TS9502	9.6	85	6	9	64	36	10	92	4	4	13
TS9512	13.8	93	2	5	70	30	14	88	3	9	31
TS9521	14.8	94	3	3	58	42	12	91	3	6	48
TS9527[c]	4.8	84	3	13	73	27	10	98	—	2	2

[a]Percentage over grass morphotypes (excluding morphotypes common to both inflorescence and leaf/stem).
[b]Percentage over the short cell morphotypes.
[c]Control sample.

https://doi.org/10.1017/S0033822200047159 Published online by Cambridge University Press

The preservation of phytoliths can be affected by their typology, as shown by Cabanes et al. (2011). For instance, inflorescence phytoliths of wheat are less stable than the phytoliths of leaves and stem. Therefore, a high number of leaf and stem phytoliths—together with a low amount of inflorescence phytoliths—might not reflect good preservation. Moreover, the so-called "weathered phytoliths" are also present in the plant itself. Thus, this parameter might not be reliable (Cabanes et al. 2011; Namdar et al. 2011).

The preservation of the assemblages under study is very good, as indicated by the presence of inflorescence phytoliths, papillae, and decorated long cells, which are among the more delicate morphotypes. Moreover, the total number of multicells compared to the control sample points to good preservation. Silica skeletons are very fragmented and include a small number of phytoliths, except for some examples (Figure 7). Morphotypes of leaf tissues are the most abundant.

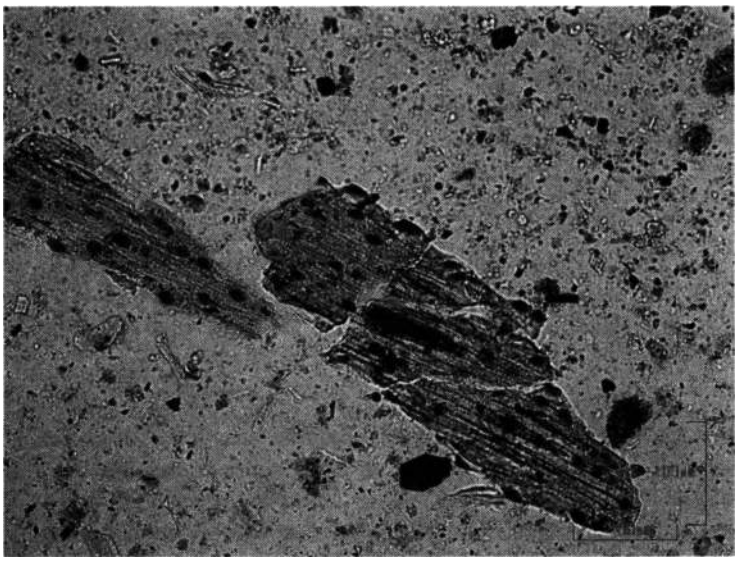

Figure 7 Leaf multicell from sample TS9512 (PPL, 20×)

Phytoliths of monocotyledonous plants are the most common morphotypes. No phytoliths of the *Cyperaceae* family (i.e. sedges) or *Phoenix* genus (i.e. palm) were identified; thus, these monocot phytoliths are most likely from grasses. The proportion of dicotyledon phytoliths is very low. The percentage of long cell dendritic single phytoliths and multicells indicates that these phytoliths are from cultivated plants. In fact, according to Albert et al. (2008), a value above 7% for dendritic phytoliths is characteristic of cultivated grass (i.e. cereal) inflorescence (Table 3).

The *Festucoideae* subfamily of the *Poaceae* true grass family is the most abundant, as represented by the percentage of rondel short cells. *Chloridoideae* and *Panicoideae* subfamilies constitute only a minor component of the assemblages analyzed. Dung spherulites and ash pseudomorphs were not identified in grain mounts, and they might have undergone postdepositional dissolution.

Micromorphology

The major mineral components observed in the thin sections are the same as those detected with FTIR. The thin sections also show the presence of phosphates (carbonated apatite) and phytoliths. Descriptions are presented in Table 4. Quartz grains, chalk fragments, and other coarse mineral

Table 4 Basic micromorphological attributes in the studied thin sections.

	Coarse fraction		Fine fraction				
Sample	Minerals/rocks/inorganic residues of biologic origin	Grain size	Ground mass	B-fabric pattern	Coarse/fine related distribution	Void types	Pedofeatures
TS9517	Quartz, subangular grains	Fine sand and silt	Reddish clay, top layer; Brown clay, bottom layer	Grano-striated	Close porphyric (dominant), open porphyric	Channels, vughs, planar, complex packing voids	Calcium carbonate crystals and intergrowths
	Chalk, fragments	From coarse sand to mm					Phosphate intergrowths
	Mollusk shells	From coarse sand to mm					
	Phytoliths	Very fine silt					
TS9526	Quartz, subangular grains	Fine sand and silt	Reddish clay, top layer; Brown clay, bottom layer	Grano-striated	Open porphyric	Channel, chambers, vughs, planar	Calcium carbonate crystals and intergrowths
	Chalk, fragments	From coarse sand to mm					Phosphate intergrowths
	Mollusk shells	From coarse sand to mm					Quartz (coarse sand size) loose infillings of planar voids
	Phytoliths	Very fine silt					

components are dispersed within a clayey matrix. Samples TS9517 and TS9526 show similar microstructures and anthropogenic components (i.e. deposited by humans), such as bone fragments, charcoal, and pottery fragments. Both samples represent an occupation surface (bottom layer), characterized by planar voids coated by phytoliths left by the decay of mudbrick straw (Figure 8). The coarse components in the upper part of the layer are organized horizontally and mixed with phosphates, which in some locations occur in a very thin lamina dividing this layer from the uppermost one. This level is covered by an accumulation of mudbrick detritus (top layer). In the case of sample TS9526, the occupation surface is sealed by a layer of phytoliths organized in a horizontal fabric, on top of which a mudbrick is visible (top layer). As shown in Figure 9, the phytolith layer and the occupational accumulation below it are rich in phosphates and anthropogenic materials. All the thin sections are consistent in showing an occupational accumulation rich in phosphates superimposed on a floor and sealed by a phytolith layer. This feature is covered by mudbrick detritus, most likely originating from the weathering of mudbrick structures such as walls. Finally, calcite ash pseudomorphs and calcareous dung spherulites were not observed in any of the slides.

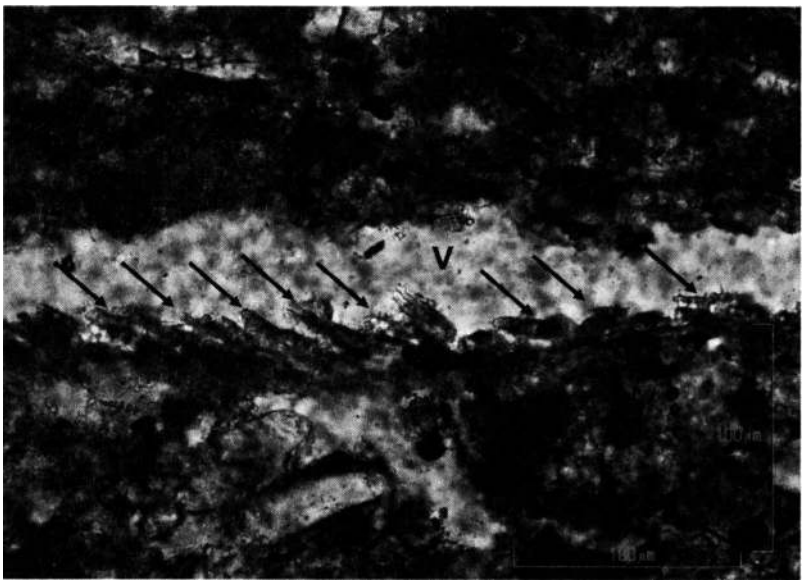

Figure 8 Microphotograph of sample TS9517, planar void (V) coated with phytoliths (marked by arrows) left by the decay of mudbrick straw (PPL, 40×).

Radiocarbon Dating

The pretreatment efficiency (i.e. the amount of sample left after the ABA protocol compared to the initial mass) ranges from 14% (RTT-6146) to 54% (RTT-6141). Different efficiency values are indicative of different states of preservation of the samples in the context under investigation. We observed that both olive pits and charcoal show a wide range of preservation states. All samples yielded a high carbon percent, between 66 to 85%, as expected for charred material.

The ^{14}C calibrated ages are presented in Table 5, with dates ordered by laboratory number. The calibrated age probability distributions are given in Figure 10. The calibrated ranges are very similar, except for the 2 oldest samples, and they cover a broad timespan from about 1400 to 1000 BCE, with little difference between the ranges based on $\pm 1\sigma$ and $\pm 2\sigma$. Remarkably, the short-lived samples yielded older ages than the charcoal, even though the latter might show an old-wood effect. Sample

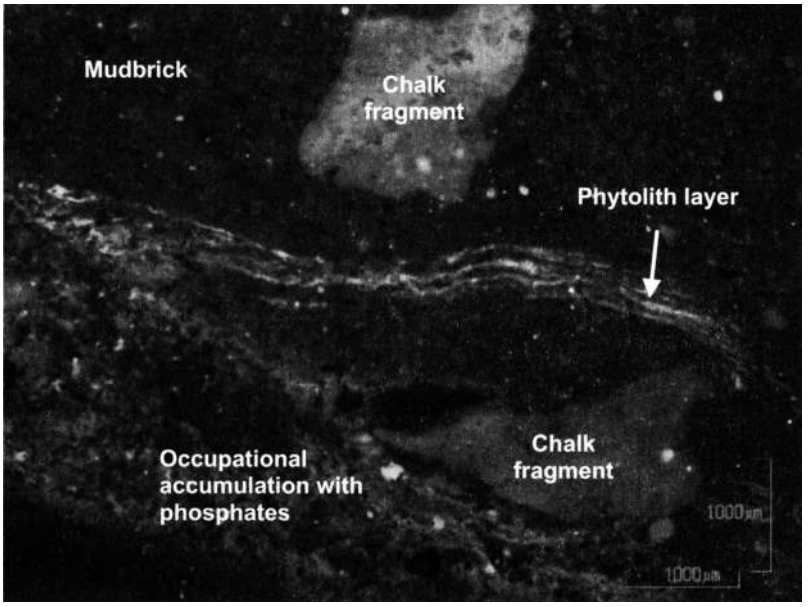

Figure 9 Microphotograph of sample TS9526, phytolith layer and associated occupational accumulation (BL, 2×). Note the high autofluorescence (yellow hue) caused by the presence of phosphates.

RTT-6139 is an olive pit from the southeast corner of Locus 126405, at the base of a Late Bronze Age wall that was reused for several decades, including during the beginning of the Iron Age (Figure 5). Therefore, we conclude that sample RTT-6139 most likely does not derive from a primary context and, therefore, is irrelevant for the purposes of this discussion.

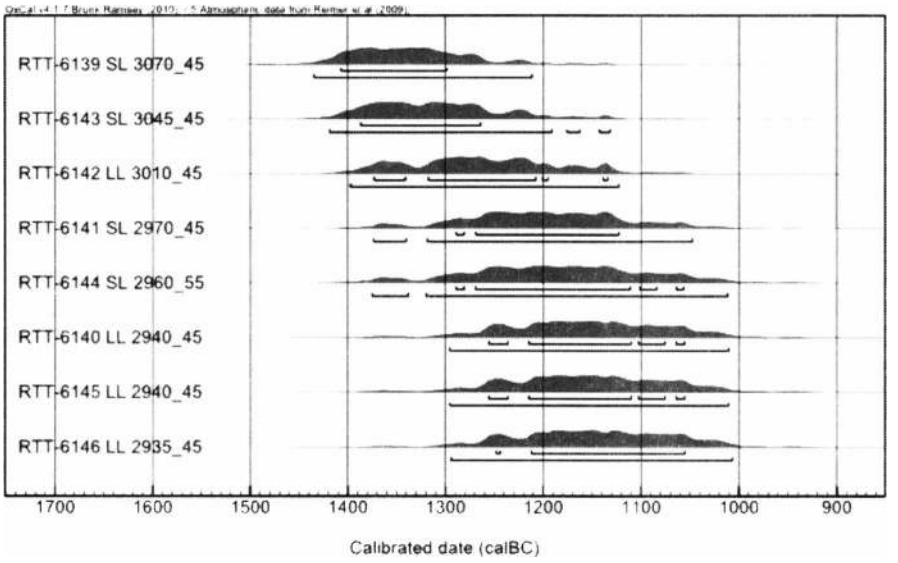

Figure 10 Probability distribution of the calibrated ages of the samples from Tell es-Safi/Gath, Area F. The samples are ordered from the oldest to the youngest (SL = short-lived sample; LL = long-lived sample).

https://doi.org/10.1017/S0033822200047159 Published online by Cambridge University Press

Table 5 ^{14}C results obtained for the samples from Tell es-Safi/Gath, Area F, Square 16C, with lab number, botanical identification, sample ID, ^{14}C age in yr BP, and calibrated ranges for $\pm 1\sigma$ and $\pm 2\sigma$. The dates are ordered by laboratory number.

RTT#	Type	Sample ID	^{14}C age ±1 yr BP	Calibrated range $\pm 1\sigma$ (BCE)	Calibrated range $\pm 2\sigma$ (BCE)
6139	Olive pit	TS9511	3070 ± 45	1410–1300 (68.2%)	1435–1210 (95.4%)
6140	Charcoal	TS9513	2940 ± 45	1255–1235 (7.5%) 1215–1110 (48.1%) 1100–1075 (9.7%) 1065–1055 (3.0%)	1295–1010 (95.4%)
6141	Olive pit	TS9521-1	2970 ± 45	1290–1280 (2.4%) 1270–1125 (65.8%)	1375–1340 (3.9%) 1320–1050 (91.5%)
6142	Charcoal	TS9521-2	3010 ± 45	1375–1340 (12.1%) 1320–1210 (52.8%) 1200–1195 (1.8%) 1140–1135 (1.5%)	1400–1125 (95.4%)
6143	Olive pit	TS9522	3045 ± 45	1385–1265 (68.2%)	1420–1190 (92.9%) 1175–1165 (1.2%) 1145–1130 (1.3%)
6144	Olive pit	TS9524	2960 ± 55	1290–1280 (2.0%) 1270–1110 (60.2%) 1100–1085 (4.3%) 1065–1055 (1.7%)	1375–1340 (4.3%) 1320–1010 (91.1%)
6145	Charcoal	TS9525	2940 ± 45	1255–1235 (7.5%) 1215–1110 (48.1%) 1100–1075 (9.7%) 1065–1055 (3.0%)	1295–1010 (95.4%)
6146	Charcoal	TS9528	2935 ± 45	1250–1245 (1.5%) 1215–1055 (66.7%)	1295–1005 (95.4%)

DISCUSSION

The most significant feature in Locus 126405 is the presence of a phytolith-rich layer covering the whole occupation surface. This surface is characterized by a high concentration of phosphates, as shown by fluorescence microscopy and by phosphate extraction. Phosphates are most likely the result of household activity (Middleton and Price 1996; Fernández et al. 2002), as suggested by the architectural features of the locus, by the presence of anthropogenic materials in thin section, and by the fact that they are concentrated within the occupational accumulation below the phytolith layer. This thin layer is composed mainly of leaf material from cultivated plants of the *Festucoideae* subfamily, which includes genera such as *Triticum* (wheat), *Hordeum* (barley), and *Secale* (rye). Wild grasses such as *Bromus* (rescue brome) and *Lolium* (ryegrass) are also common to the region of the Shephelah/Judean Foothills (Danin 2004; Figure 1), and could well be part of the assemblages analyzed. This evidence indicates that the phytolith layer originated from the decay of a mat, or more simply a vegetal cover for the floor, made of parts of cultivated plants (straw/chaff), rather than from the accumulation of animal dung in an enclosure (Shahack-Gross et al. 2005; Albert et al. 2008). The absence of calcareous dung spherulites (Canti 1999) supports this point, even though they might have dissolved after their deposition. However, the amount of calcite within the sediments, as shown by FTIR spectrometry, points to good preservation of this component.

Although ash pseudomorphs were not identified in grain mounts, some of the samples analyzed with FTIR might contain dispersed calcite in the form of ash, according to the calcite grinding curve method proposed by Regev et al. (2010a). It has been observed (M Toffolo, unpublished data) that a mixture of 50% ash and 50% chalk yields an FTIR signal characteristic of ash. However, further investigation is needed regarding grinding curves of mixed materials.

The olive pits and charcoal fragments collected from Locus 126405 thus derive from a well-defined domestic occupational accumulation, with a specific pottery assemblage, which can be considered as a good context for ^{14}C dating. Nevertheless, the range of the calibrated ages is very wide (mainly due to the nature of the calibration curve) and short-lived samples show older ages compared to charcoal.

If we consider that the ^{14}C samples were deposited as a result of a single depositional event and we consequently average the dates, the timespan obtained covers the period 1269–1126 BCE for the ±2σ range (Figure 11), which is half of the period covered by the calibrated probability distribution of the single dates (the ±1σ range is almost identical). However, this is an arbitrary decision, since the relationship between the samples is unknown, and they might have been deposited at different times. We therefore plotted these ^{14}C dates with OxCal according to other constraints, namely in a phase and in a sequence, to estimate the start and end dates for Locus 126405. In the first case (Figure 12), the phase has by definition no internal order; thus, the software will try to accommodate each date in order to fit the model. Of course, this operation results in a very "compacted" model, in which the timespan allotted to the phase is kept at a minimum. The ±2σ range for the beginning of the phase is 1400–1140 BCE, whereas for the end is 1260–1020 BCE. The Bayesian model in Figure 13 shows the dates organized within a sequence, which by definition must have a criterion for the internal ordering of the dates. In this case, since there is no available information regarding the stratigraphic relationship between the different samples, the criterion we decided to use is the chronological order of the uncalibrated dates, from the oldest to the youngest (which is arbitrary). The ±2σ range for the beginning of the sequence is 1475–1160 BCE, whereas for the end is 1250–960 BCE.

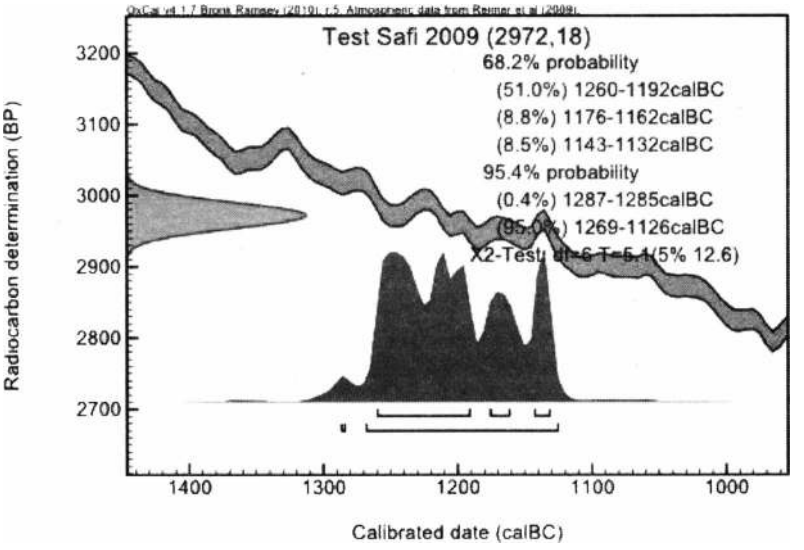

Figure 11 Dates from Tell es-Safi/Gath (excluding sample RTT-6139) combined together. Note that the results pass the χ^2 test.

https://doi.org/10.1017/S0033822200047159 Published online by Cambridge University Press

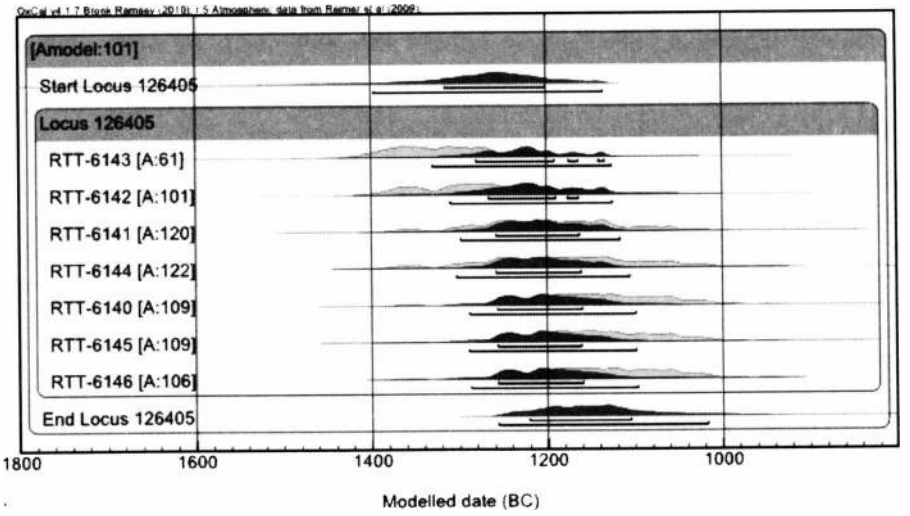

Figure 12 Bayesian model of dates from Tell es-Safi/Gath (excluding sample RTT-6139) organized within a phase.

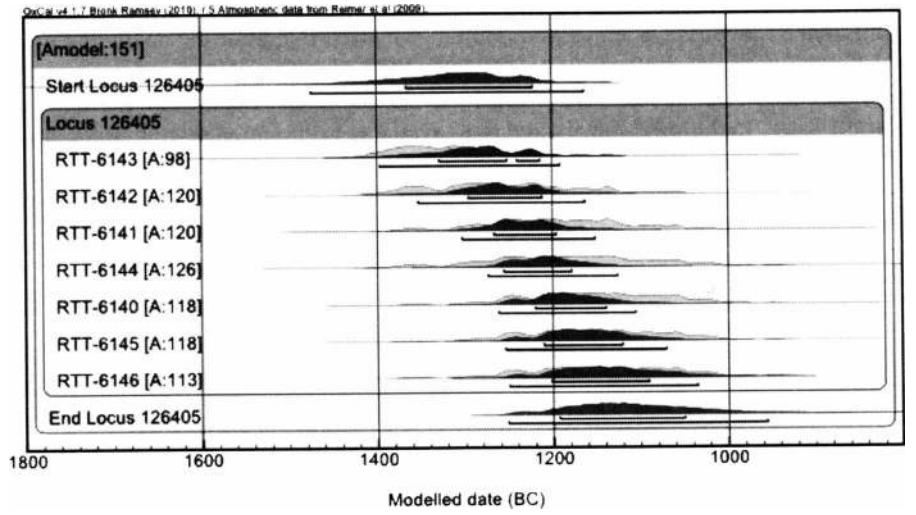

Figure 13 Bayesian model of dates from Tell es-Safi/Gath (excluding sample RTT-6139) organized within a sequence.

These 2 models show a good agreement and similar results, with the phase being slightly compacted compared to the sequence, on the order of ~60 calendar years. However, the timespan covered by Locus 126405 remains wide and centered on 1200–1170 BCE, thus confirming the relative chronology given by the pottery assemblage and with no possibility of supporting the HC or the LC. This means that, despite the internal order of the samples within the context, it is not possible to obtain a high-precision date. From a stratigraphic point of view, to know the relative chronological relationship among these samples would not decrease the timespan covered. Furthermore, the wiggles and flat regions of the calibration curve constitute a major problem for the Late Bronze Age and early Iron Age I period, affecting the precision of the dates.

Besides the relationships between the different samples, also the mode of deposition of Locus 126405 plays an important role, as indicated by the fact that short-lived samples show older dates compared to the long-lived ones. This can be explained in 2 ways. First, Area F is located on a very steep slope, and it is likely that colluvium from the top rolled down the hill, thus mixing older and younger material. It is not possible to state whether this happened during the occupation of this locus or after its abandonment. Secondly, it is possible that Locus 126405 underwent a long-term sedimentation process that led to the deposition of allochthonous material, either younger or older. We believe that this is the most relevant factor because of the preservation of the intact phytolith layer, which indicates no later remixing of the sediments, and the slight changes in ceramic typologies through time. This in turn indicates that each of the samples dated should be regarded as being the result of different depositional events, and that the dates should not be averaged, even in the case of an accumulation on a floor, which in stratigraphic terms is considered as a single event and, therefore, is supposed to contain contemporary materials. Hence, in order to address chronological issues that require high-precision and high-accuracy dating, only clusters of short-lived samples should be processed. Samples occurring in clusters are more likely to be deposited altogether in a specific moment and allow for several measurements of the same material, which can then be averaged. The analysis of several clusters of short-lived samples retrieved from secure contexts deposited in sequence and characterized through a microarchaeological approach could significantly improve the dating of the Bronze Age/Iron Age transition, which is affected by a plateau in the calibration curve, and of the various phases of the Iron Age, thus contributing to add new data to the ongoing debate on the Iron Age chronology of the southern Levant.

CONCLUSION

The ^{14}C determinations from Area F in Tell es-Safi/Gath place the end of the Philistine Monochrome phase within the $\pm 1\sigma$ range of 1400–1050 BCE. The locus from which the samples for ^{14}C dating were collected was thoroughly investigated in order to ascertain the integrity and function of the context. Locus 126405 proved to be a domestic occupation surface in primary deposition characterized by the presence of a well-preserved phytolith-rich layer. The broad timespan of this context is most probably the result of the mixing of old and young single fragments of charred material within the same locus, caused by a long-term sedimentation process. For this reason, only clusters of short-lived samples coming from several locations within the same stratigraphic sequence should be considered in order to solve chronological issues that require high resolution in the presence of plateaus in the calibration curve. Finally, we strongly advocate the application of a microarchaeological approach to the study of archaeological contexts for ^{14}C dating.

ACKNOWLEDGMENTS

We wish to thank Dr Eric Welch for his invaluable help during fieldwork, Dr Dan Cabanes i Cruelles and Yotam Asscher for important comments, and Eugenia Mintz for her assistance during laboratory work. The excavations at Tell es-Safi/Gath are conducted under the auspices of Bar-Ilan University and are directed by AMM. The research leading to these results has received funding from the European Research Council under the European Community's Seventh Framework Programme (FP7/2007-2013)/ERC grant agreement n° 229418. This research was also supported by a grant to AMM from the German-Israel Foundation for Science and Research (grant # 132/2009).

REFERENCES

Albert RM, Shahack-Gross R, Cabanes D, Gilboa A, Lev-Yadun S, Portillo M, Sharon I, Boaretto E, Weiner S. 2008. Phytolith-rich layers from the Late Bronze and Iron Ages at Tel Dor (Israel): mode of formation and archaeological significance. *Journal of Archaeological Science* 35(1):57–75.

Bachhuber C, Roberts R. 2009. *Forces of Transformation: The End of the Bronze Age in the Mediterranean.* Proceedings of an International Symposium Held at St. John's College, University of Oxford, 25–26 March 2006. Oxford: Oxbow.

Berna F, Behar A, Shahack-Gross R, Berg J, Boaretto E, Gilboa A, Sharon I, Shalev S, Shilstein S, Yahalom-Mack N, Zorn JR, Weiner S. 2007. Sediments exposed to high temperatures: reconstructing pyrotechnological processes in Late Bronze and Iron Age strata at Tel Dor (Israel). *Journal of Archaeological Science* 34(3): 358–73.

Boaretto E. 2007. Determining the chronology of an archaeological site using radiocarbon: minimizing uncertainty. *Israel Journal of Earth Sciences* 56(2/4): 207–16.

Boaretto E. 2009. Dating materials in good archaeological contexts: the next challenge for radiocarbon analysis. *Radiocarbon* 51(1):275–81.

Boaretto E, Jull AJT, Gilboa A, Sharon I. 2005. Dating the Iron Age I/II transition in Israel: first intercomparison results. *Radiocarbon* 47(1):39–55.

Bronk Ramsey C. 2009. Bayesian analysis of radiocarbon dates. *Radiocarbon* 51(1):337–60.

Bruins HJ, van der Plicht H, Mazar A. 2003. ^{14}C dates from Tel Rehov: Iron-Age chronology, pharaohs, and Hebrew kings. *Science* 300(5617):315–8.

Bruins HJ, Nijboer AJ, van der Plicht H. 2011. Iron Age Mediterranean chronology: a reply. *Radiocarbon* 53(1):199–220.

Bullock P, Fedoroff N, Jongerius A, Stoops G, Tursina T, Babel U. 1985. *Handbook for Soil Thin Section Description.* Albrighton: Waine Research Publications.

Cabanes D, Weiner S, Shahack-Gross R. 2011. Stability of phytoliths in the archaeological record: a dissolution study of modern and fossil phytoliths. *Journal of Archaeological Science* 38(9):2480–90.

Canti MG. 1999. The production and preservation of faecal spherulites: animals, environment and taphonomy. *Journal of Archaeological Science* 26(3):251–8.

Carmi I, Ussishkin D. 2004. ^{14}C dates. In: Ussishkin D, editor. *The Renewed Archaeological Excavations at Lachish (1973–1994).* Tel Aviv.

Chu V, Regev L, Weiner S, Boaretto E. 2008. Differentiating between anthropogenic calcite in plaster, ash and natural calcite using infrared spectroscopy: implications in archaeology. *Journal of Archaeological Science* 35(4):905–11.

Courty MA, Goldberg P, Macphail RI. 1989. *Soils and Micromorphology in Archaeology.* Cambridge: Cambridge University Press.

Danin A. 2004. *Distribution Atlas of Plants in the* Flora Palaestina *Area.* Jerusalem: The Israel Academy of Sciences and Humanities.

Dothan T, Zukerman A. 2004. A preliminary study of the Mycenaean IIIC: pottery assemblages from Tel Miqne-Ekron and Ashdod. *Bulletin of the American Schools of Oriental Research* 333:1–54.

Dothan T, Gitin S, Zukerman A. 2006. Chapter 3. The pottery: Canaanite and Philistine traditions and Cypriot and Aegean imports. In: Meehl M, Dothan T, Gitin S, editors. *Tel Miqne-Ekron Excavations 1995–1996: Field INE East Slope, Iron Age I (Early Philistine Period).* Jerusalem: WF Albright Institute of Archaeology. p 71–175.

Eliyahu-Behar A, Yahalom-Mack N, Shilstein S, Zukerman A, Shafer-Elliott C, Maeir AM, Boaretto E, Finkelstein I, Weiner S. 2012. Iron and bronze production in Iron Age IIA Philistia: new evidence from Tell es-Safi/Gath, Israel. *Journal of Archaeological Science* 39(2):255–67.

Fantalkin A, Finkelstein I, Piasetzky E. 2011. Iron Age Mediterranean chronology: a rejoinder. *Radiocarbon* 53(1):179–98.

Fernández FG, Terry RE, Inomata T, Eberl M. 2002. An ethnoarchaeological study of chemical residues in the floors and soils of Q'eqchi' Maya Houses at Las Pozas, Guatemala. *Geoarchaeology* 17(6):487–519.

Finkelstein I. 1996. The archaeology of the United Monarchy: an alternative view. *Levant* 28:177–87.

Finkelstein I, Piasetzky E. 2007. Radiocarbon dating and Philistine chronology with an addendum on el-Ahwat. *Egypt and the Levant* XVII:73–82.

Finkelstein I, Piasetzky E. 2010. Radiocarbon dating the Iron Age in the Levant: a Bayesian model for six ceramic phases and six transitions. *Antiquity* 84(324): 374–85.

Gitin S, Mazar A, Stern E. 1998. *Mediterranean Peoples in Transition: Thirteenth to Early Tenth Centuries BCE.* Jerusalem: Israel Exploration Society.

Goldberg P, Berna F. 2010. Micromorphology and context. *Quaternary International* 214(1–2):56–62.

Goldberg P, Macphail RI. 2006. *Practical and Theoretical Geoarchaeology.* Malden: Blackwell Publishing.

Harrison T. 2006–2007. *Cyprus, the Sea Peoples and Eastern Mediterranean: Regional Perspectives of Continuity and Change.* Toronto: Canadian Institute for Mediterranean Studies.

Holliday VT, Gartner WG. 2007. Methods of soil P analysis in archaeology. *Journal of Archaeological Science* 34(2):301–33.

Katz O, Cabanes D, Weiner S, Maeir AM, Boaretto E, Shahack-Gross R. 2010. Rapid phytolith extraction for analysis of phytolith concentrations and assemblages during an excavation: an application at Tell es-Safi/Gath, Israel. *Journal of Archaeological Science* 37(7):1557–63.

Killebrew A. 2005. *Biblical Peoples and Ethnicity: An Archaeological Study of Egyptians, Canaanites, Philistines, and Early Israel 1300–1100 BCE.* Atlanta: Society of Biblical Literature.

Madella M, Alexandre A, Ball T. 2005. International Code for Phytolith Nomenclature 1.0. *Annals of Botany* 96:253–60.

Maeir AM. 2005. Philister-Keramik. In: Frantz-Szabo G, Hellwag U, editors. *Reallexikon der Assyriologie und vorderasiatischen*. Archäologie Band 14. Berlin: W de Gruyter.

Maeir AM. 2008. Zafit, Tel. In: Stern E, editor. *The New Encyclopedia of Archaeological Excavations in the Holy Land 5: Supplementary Volume*. Jerusalem: Israel Exploration Society. p 2079–81.

Maeir AM. 2012. Chapter 1: The Tell es-Safi/Gath Archaeological Project 1996–2010: Introduction, Overview and Synopsis of Results. In: Maeir AM, editor. *Tell es-Safi/Gath I: Report on the 1996–2005 Seasons*. Wiesbaden: Harrassowitz.

Mazar A, Carmi I. 2001. Radiocarbon dates from Iron Age strata at Tel Beth Shean and Tel Rehov. *Radiocarbon* 43(3):1333–42.

Mazar A, Bruins H, Panitz-Cohen N, van der Plicht H. 2005. Ladder of time at Tel Rehov: stratigraphy, archaeological context, pottery and radiocarbon dates. In: Levy TE, Higham T, editors. *The Bible and Radiocarbon Dating: Archaeology, Text and Science*. London: Equinox. p 193–255.

Middleton WD, Price TD. 1996. Identification of activity areas by multi-element characterization of sediments from modern and archaeological house floors using inductively coupled plasma-atomic emission spectroscopy. *Journal of Archaeological Science* 23(5): 673–87.

Mulholland SC, Rapp GJ. 1992. Phytolith systematics: an introduction. In: Mulholland SC, Rapp GJ, editors. *Phytolith Systematics: Emerging Issues*. New York: Plenum Press. p 1–13.

Namdar D, Zukerman A, Maeir AM, Katz JC, Cabanes D, Trueman C, Shahack-Gross R, Weiner S. 2011. The 9th century BCE destruction layer at Tell es-Safi/Gath, Israel: integrating macro- and microarchaeology. *Journal of Archaeological Science* 38(12):3471–82.

Olson EA, Broecker WS. 1958. Sample contamination and reliability of radiocarbon dates. *Transactions of the New York Academy of Science Series* II 20:593–604.

Oren E. 2000. *The Sea Peoples and Their World: A Reassessment*. Philadelphia: University Museum.

Piperno DR. 1988. *Phytolith Analysis: An Archaeological and Geological Perspective*. San Diego: Academic Press.

Piperno DR. 2006. *Phytoliths: A Comprehensive Guide for Archaeologists and Paleoecologists*. Lanham: AltaMira Press.

Poduska KM, Regev L, Boaretto E, Addadi L, Weiner S, Kronik L, Curtarolo S. 2011. Decoupling local disorder and optical effects in infrared spectra: differentiating between calcites with different origins. *Advanced Materials* 23(4):550–4.

Rebollo NR, Cohen-Ofri I, Popovitz-Biro R, Bar-Yosef O, Meignen L, Goldberg P, Weiner S, Boaretto E. 2008. Structural characterization of charcoal exposed to high and low pH: implications for ^{14}C sample preparation and charcoal preservation. *Radiocarbon* 50(2): 289–307.

Regev L, Poduska KM, Addadi L, Weiner S, Boaretto E. 2010a. Distinguishing between calcites formed by different mechanisms using infrared spectrometry: archaeological applications. *Journal of Archaeological Science* 37(12):3022–9.

Regev L, Zukerman A, Hitchcock L, Maeir AM, Weiner S, Boaretto E. 2010b. Iron Age hydraulic plaster from Tell es-Safi/Gath, Israel. *Journal of Archaeological Science* 37(12):3000–9.

Reimer PJ, Baillie MGL, Bard E, Bayliss A, Beck JW, Blackwell PG, Bronk Ramsey C, Buck CE, Burr GS, Edwards RL, Friedrich M, Grootes PM, Guilderson TP, Hajdas I, Heaton TJ, Hogg AG, Hughen KA, Kaiser KF, Kromer B, McCormac FG, Manning SW, Reimer RW, Richards DA, Southon JR, Talamo S, Turney CSM, van der Plicht J, Weyhenmeyer CE. 2009. IntCal09 and Marine09 radiocarbon age calibration curves, 0–50,000 years cal BP. *Radiocarbon* 51(4): 1111–50.

Rypkema HA, Lee WE, Galaty ML, Haws J. 2007. Rapid, in-stride soil phosphate measurement in archaeological survey: a new method tested in Loudoun County, Virginia. *Journal of Archaeological Science* 34(11):1859–67.

Shahack-Gross R. 2011. Herbivorous livestock dung: formation, taphonomy, methods for identification, and archaeological significance. *Journal of Archaeological Science* 38(2):205–18.

Shahack-Gross R, Albert R-M, Gilboa A, Nagar-Hilman O, Sharon I, Weiner S. 2005. Geoarchaeology in an urban context: the uses of space in a Phoenician monumental building at Tel Dor (Israel). *Journal of Archaeological Science* 32(9):1417–31.

Sharon I, Gilboa A, Jull AJT, Boaretto E. 2007. Report on the first stage of the Iron Age dating project in Israel: supporting a low chronology. *Radiocarbon* 49(1):1–46.

Stoops G. 2003. *Guidelines for Analysis and Description of Soil and Regolith Thin Sections*. Madison: Soil Science Society of America.

Stuiver M, Polach HA. 1977. Discussion: reporting of ^{14}C data. *Radiocarbon* 19(3):355–63.

Twiss PC, Suess E, Smith RM. 1969. Morphological classification of grass phytoliths. *Soil Science Society of America* 33:109–15.

van der Plicht H, Bruins HJ. 2001. Radiocarbon dating in Near-Eastern contexts: confusion and quality control. *Radiocarbon* 43(3):1155–66.

van der Plicht H, Bruins HJ, Nijboer AJ. 2009. The Iron Age around the Mediterranean: a High Chronology perspective from the Groningen radiocarbon database. *Radiocarbon* 51(1):213–42.

Ward WA, Sharp Joukowsky M, Astrom P. 1992. *The Crisis Years: The 12th Century B.C. – From Beyond the Danube to the Tigris*. Dubuque: Kendall/Hunt.

Weiner S. 2010. *Microarchaeology. Beyond the Visible Archaeological Record*. Cambridge: Cambridge University Press.

Yasur-Landau A. 2010. *The Philistines and Aegean Migration at the End of the Late Bronze Age*. Cambridge: Cambridge University Press.

Yizhaq M, Mintz G, Cohen I, Khalaily H, Weiner S, Boaretto E. 2005. Quality controlled radiocarbon dating of bones and charcoal from the early Pre-Pottery Neolithic B (PPNB) of Motza (Israel). *Radiocarbon* 47(2):193–206.